INFERENTIAL MINING FOR RECONSTRUCTION OF 3D CELL STRUCTURES IN ATOMIC FORCE MICROSCOPY IMAGING

Mario d'Acunto[1], Stefano Berrettini[2], Serena Danti[2], Michele Lisanti[3], Mario Petrini[4],
Andrea Pietrabissa[5] and Ovidio Salvetti[1]

[1]*Istituto di Scienze e Tecnologia dell'Informazione, ISTI-CNR, via Moruzzi 1, I-56124, Pisa, Italy*

[2]*Dept. of Neuroscience, University of Pisa, via Roma 55, 56126, Pisa, Italy*
[3]*Dept. of Orthopedics &Traumatology, University of Pisa, via Paradisa 2, 56124, Pisa, Italy*
[4]*Dept. of Oncology & Transplants, University of Pisa, via Roma 55, 56126, Pisa, Italy*
[5]*Dept. of Surgical Sciences, IRCCS Policlinico San Matteo, University of Pavia, 27100 Pavia, Italy*

Keywords: Atomic Force Microscopy imaging, 3D cell reconstruction, Bayesian single frame high-resolution.

Abstract: Atomic Force Microscopy (AFM) is a fundamental tool for the investigation of a wide range of mechanical properties on nanoscale due to the contact interaction between the AFM tip and the sample surface. The focus of this paper is on an algorithm for the reconstruction of 3D stem-differentiated cell structures extracted by typical 2D surface AFM images. The AFM images resolution is limited by the tip-sample convolution due to the combined geometry of the probe tip and the pattern configuration of the sample. This limited resolution limits the accuracy of the correspondent 3D image. To drop unwanted effects, we adopt an inferential method for pre-processing single frame AFM image (low resolution image) building its super-resolution version. Therefore the 3D reconstruction is made on animal cells using a Markov Random Field approach for augmented voxels. The 3D reconstruction should improve unambiguous identification of cells structures. The computation method is fast and can be applied both to multi- and to single-frame images.

1 INTRODUCTION

In this paper, we adopt an inferential procedure providing a high-resolution algorithm for the single-image AFM raw data and then the construction of a 3D routine for the improved resolution images. When applied to cell populations, the 3D reconstruction, as developed in this paper, is a useful tool for the recognition of cell patterns and organs and it could be used for a fast *in situ* analysis for biologists and biomedical scientists.

In the last two decades, AFM has been developed well beyond the topographic imaging tool. It has become an important instrument for manipulation and material property characterizations at the nanometer scale. The precision of positioning has always been the key driver for AFM technology and scanning probe microscopy in general. Nevertheless, uncontrolled hardware drift, such as piezo creep and thermal drift, can cause image distortion and limiting resolution. Some solutions based on offline corrections (Yurov and Klimov, 1994), hardware optimization (Hug et al., 1992;

Altmann et al., 2000; Beyder et al., 2006), image based real-time compensation (Clayton and Devasia, 2005), or image-based adaptive control has been proposed (Belikov et al., 2008; D'Acunto and Salvetti, 2011). An AFM probe tip measures the topography of a surface by looking the vertical deflection of a cantilever and then associating a z-height value to the correspondent vertical deflection. The resulting image is obtained plotting the function $z_i=f(x_i,y_i)$, for any couple (x_i,y_i) of the sample surface. The focus of this paper is to build a method for a 3D reconstruction after the acquired AFM image is processed in order to obtain its High-Resolution (HR) representation.

HR methods are techniques that enhance the resolution of an imaging system. In optical based imaging, HR techniques break the diffraction-limit, analogously, HR methods can improve the resolution of digital imaging sensors. HR techniques can be divided in two categories, single-frame or multiple-frame, respectively. Multiple-frame HR use the sub-pixel shifts between multiple low resolution images of the same scene. On the contrary, single

frame HR methods attempt to magnify the image without introducing blur. These last methods use other parts of the low resolution images to make an extimation on what the high resolution images should look like. AFM imaging requires to work using a single-frame approach: given a single image of sample scanned at low resolution, return the image that is mostly likely to be generated from a noiseless high resolution scan of the same sample portion. After HR equilavent image is reached, 3D recostruction is made possible using a Markov Random Field (MRF) approach. In a MRF method we consider a couple (h_m, N), where a stochastic process is indexed by an augmented voxel h_m for which, for every couple (x,y) of the 2D image, any augmented voxel depends only on its immediate neighbours of the N set, where N is a parameter space. The choice of N depends by the system variables conditional probability distributions, where system variables provide the basic tool for modelling spatial continuity.

We apply our method to cells derived by stem primitive cells and differentiated in osteocytes or adipocytes, or fibroblast. Any differentiated stem cell develops specific organs and functions, and recognition such organs is not a trivial question. The 3D reconstruction is useful when does not lose information of the primitive image and gives the possibility to identify unambiguous such specific organs.

2 INFERENTIAL GENERATIVE MODEL

Despite the AFM ability to reach high spatial resolution, the acquired surface topography image can sometimes not correspond to the real surface features due to the effect of the instrument on the object producing artefacts. These artefacts can be generally taken into consideration while qualitatively interpreting the AFM results. However, 3D reconstruction tools require quantitative estimation and reconstruction of sample true geometry. During scanning, two major AFM artefacts can appear: a profile broadening effect due to the tip-sample convolution and the height lowering effect due to the elastic deformation of studied samples.

The first effect can be schematised as follows: the tip moving across an object surface can be approximated by a sphere of radius R moving along a sphere of radius r surface, i.e., the tip describes arc of radius $R+r$. The lateral dimension of the surface

objects is $r_c = 2(R \cdot r)^{1/2}$ and the relative height of the object

$$\Delta z = r[1 - (1 - (r_c/(R+r))^2] \qquad (1)$$

The minimum separation between two asperities or local pattern that can be detected is $d = (8R\Delta z)^{1/2}$, that is also the lateral resolution.

Before to build the 3D structures, the source images are processed in order to improve their resolution. To do this operation, we adopt a Bayesian method. Hardie et al (Hardie et al, 1997) demonstrated that low-resolution images can be updated using super-resolution image estimate, and that this improves a *Maximum a Posteriori* (MAP) super-resolution image estimate. Pickup et al. (Pickup et al., 2009) used a similar joint MAP approach to learn more general geometric patterns, configuring the correspondent super-resolution images and valuing the prior parameters simultaneously. Another remarkable result for the inferential super-resolution has been reached by Tipping and Bishop (Tipping and Bishop, 2003), they used a Maximum Likelihood (ML) point estimate of the image parameters found by integrating the high-resolution image out the registration problem and optimising the marginal probability of the observed low-resolution images directly.

We follow a generative model based on an idea as proposed by Torres-Mendez et al. (Torres-Mendez et al., 2007) carried out from single-frame methods. The basic idea can be summarized as follows: given a Low Resolution (LR) image α of size $h_\alpha \times w_\alpha$ pixels, we want to estimate the correspondent HR image ω of size $h_\omega \times w_\omega$, with equal or greater size of the input image α. From α, we must generate L images of smaller size (scaled), that we can call observable images l, with $l=0…L$. Any point in the LR image is considered as a node in a Markovian process, and a possible neighbourhood node in the HR image is defined by a pairwise potential. If we denote x_i as a set of hidden nodes in the output ω, and the y_i as the observable nodes in α image, and defining the pairwise potential between the variables x_i, and x_j, by Ψ_{ij} and the local evidence potential associated with the variables x_i and y_j by Φ_i, the joint probability correspondent to the Markovian process can be written as

$$P(x,y) = \frac{1}{Z} \prod_{i,j} \psi_{ij}(x_i, x_j) \prod_i \Phi_i(x_i, y_i) \qquad (2)$$

where Z is a normalization constant. Our problem consists to maximize $P(x,y)$, maximization that corresponds to find the most likely state for all hidden nodes x_i, given all the node y_i. To remove

ambiguities, we decide to assign high compatibility between neighbouring pixels that have similar intensity values and low compatibility between neighbouring pixels that present drastic changes in their intensity values. The value of any single pixel in HR ω image is obtained estimating the maximum *a posteriori* (MAP) solution associated to the MRF model as given by eq. (2)

$$\omega_{MAP} = \arg\max_{\omega} P(\omega|\alpha) \qquad (3)$$

where

$$P(\omega|\alpha) \propto P(\alpha|\omega)P(\omega) \propto$$
$$\prod_{i,j} \psi_{ij}(x_i, x_j) \prod_i \Phi_i(x_i, y_i) \qquad (4)$$

Being the conditional probabilities impossible to be exactly computed, because it is impossible to represent all the possible combinations between pixels, we adopt a Markov Chain Monte Carlo (MCMC) method to approximate the best solution of (3). The HR images so obtained are still 2D representation of the acquired AFM images. The correspondent 3D reconstruction is discussed in the next section

3 3D RECONSTRUCTION MODEL

The typical visual rendering of AFM images describes the recorded structures assessing a gray intensity (o colour intensity) to the $z=f(x,y)$ measured value. This is not properly a 3D reconstruction. 3D reconstruction is possible in tomography-based techniques thanks to the multi-acquisition of images at different angles and then recollected in a unique image via Radon anti-transformation, for example. When the source is composed by a unique image, the 3D reconstruction is rather complicated, and the possibility to introduce artefacts or unwanted effects is high. Our method is based on learning a statistical model of the local relationship between the observed range data and the variations in the intensity image and uses this model to compute unknown depth values. The intensity of any point is supposed to be a Markov process. Unknown depth values are then inferred by using the statistics of the observed range data to determine the behaviour of the Markov process. The presence of intensity where range data is being inferred is crucial since intensity provides knowledge of surface smoothness and variations in depth. The advantage of our approach is to carry out knowledge directly from the observed data, without

to introduce constraints that could be inapplicable to particular environments. Although if our method seem to be very close to a traditional shape-from-shading method (where depth inference from variations in surface shading), the substantial difference is in the inferential engine that connects the final 3D reconstruction to a suitable processing of original data.

3.1 Reconstruction Methodology

Our goal is to infer a dense range map from an intensity image and a very sparse initial range data. The inference on range data is solved using a sampling on the intensity at each point considered as a product of a Markovian process. Unknown range data is then inferred by using the statistics of the observed range data to determine the behaviour of the Markovian process. In our approach, there some critical aspects, for example, the knowledge extracted from smooth intensity variation could generate artefacts, or again, the right weight of a variation in depth.

The starting point is the development of a set of augmented voxels V that contain intensity, edge (from the intensity range) and range information. It should be mentioned that the intensity can be considered both for gray scales or colour images, and that the range information includes portion of ranges a priori unknown). Let us introduce Ω as the area of unknown range that corresponds to the region to be filled. Following Torres-Mendez et al. (Torres-Mendes et al, 2007), we base our reconstruction method on the amount of reliable information surrounding the augmented voxel whose depth value is to be estimated, and also on the edge information. Thus, for each augmented voxel V_i we count the number of neighbour voxels with already assigned range and intensity. A general criterion is to start by reconstructing those augmented voxels which have more of their neighbour voxels already filled, leaving to the end those with an edge passing through them. After a depth value is estimated, we update each of its neighbours by adding 1 to their own neighbour counters. The next step is to proceed to the subsequent groups of augmented voxels to synthesise until no more augmented voxels in Ω exists.

Formally, an augmented voxel is defined as $V=(z,E,R)$ where z denotes the pixel intensity directly connected to the z-height as measured by the AFM, E is a binary matrix (1 if an edge exits, 0 otherwise) and R denotes the matrix of incomplete pixels depth. It is possible to define a set of

augmented voxels that lie on each ray that intersects each pixel of the input image z, thus giving us a registered range image R and intensity image z. Let $h_m=(x,y)$: $1\leq x,y\leq m$ denote the m integer lattice , then $z=\{z_{x,y}\}$, $(x,y)\in h_m$, denotes the gray levels of the input image, and $r=\{R_{x,y}\}$, denotes the depth values. Than we model the V set as a Markov Random Field. Within the Markov Random Field picture, z and R must be considered random variables. Let us introduce a neighbourhood system, defined as $N=\{N_{x,y}\in h_m\}$, where $N_{x,y}\subset h_m$ denotes the neighbours of (x,y).

A Markov Random Field over (h_m, N) is a stochastic process indexed by h_m for which, for every couple (x,y) any augmented voxel depends only on its immediate neighbours. The choice of N together with the conditional probability distribution of $P(z)$ and $P(R)$ provides the basic tool for modelling spatial continuity. Therefore, the $N_{x,y}$ set is modelled on the acquisition data matrix that is a square mask of size $n\times n$ centered at the augmented voxel location (x,y). The calculation of the conditional probabilities in an explicit form is an infeasible task since we cannot efficiently represent or determine all the possible combinations between augmented voxels with its associated neighbours. To do this calculation we can invoke the Gibbs sampling, for example, and average a depth value from the augmented voxel $V_{x,y}$ with neighbours $N_{x,y}$ by selecting range value from the augmented resembles the region being filled voxel whose neighbours $N_{k,l}$ most resembles the region being filled in

$$N_{opt} = \arg\min_{(k,l)\in A}\left\|N_{x,y} - N_{k,l}\right\| \qquad (5)$$

where $A=\{A_{k,l}\subset N\}$ is the set of local neighborhood, in which the center voxel has already assigned a depth value, such that $1\leq[(k\text{-}x)^2+(l\text{-}y)^2]^{1/2}\leq d$. For each successive augmented voxel, N_{opt} as given by Eq. (5) approximates the maximum a posteriori estimate. The distance $\|\cdot\|$ is defined as the weighted sum of squared differences over the partial data in two neighbourhoods. The weights are choice applying 2D Gaussian kernel to each neighbourhood, such that those voxels near the center are given more weight than those at the edge of the window.

4 RESULTS

In this section, we present the basic results inherent the 3D model as discussed in the past two sections.

The primitive AFM images are processed in order to improve their quality (ranging from LR to HR) and then the algorithm for their 3D reconstruction using the MRF picture as given by Eq. (5) is applied. Firstly, the method is used on images of regular lattice for AFM calibration to sample with nanometers patterns. Figure 1 shows silicon grating, normally used for calibration of z-height in AFM measurements. Its accurate 3D reconstruction of the grains is of great importance. It should be noted that the image in figure 1 has not been pre-processed and it presents an artefact at the bottom, while the image in figure 3 that represents its correspondent 3D reconstruction corrects such artefact.
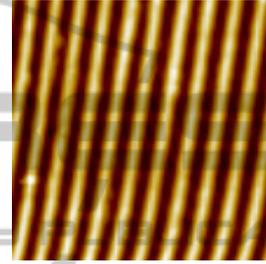

Figure 1: Silicon grating used for AFM calibration of z-height. The mounds are large 100nm and periodicity is 200nm.
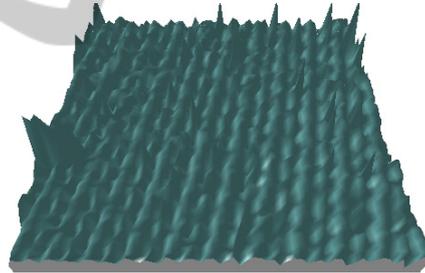

Figure 2: 3D reconstruction of the image as in figure 1 without HR processing of the 2D image. Some artefacts and topographic roughness present in the primitive 2D image are amplified and the grating is not well resolved.
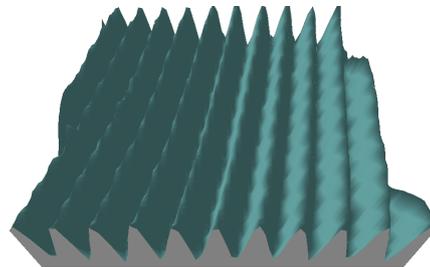

Figure 3: 3D reconstruction of the grating as in figure 1 with HR processing applied on the image as recorded by the AFM. In this case, the artefacts are removed and the grating presents a spatially well-resolved structure, where mounds and valleys are clearly separated.

Now, we apply our procedure to cell images. The cell samples are obtained in cellular cultures from pluripotent stem cells and differentiated in osteocytes, fibroblasts, adipocytes or others (Danti et al. 2006).

A typical problem acquiring images on cells using an AFM is the low resolution due large dimensions of cells and reduced instrumental capability to increase pixels. For example, many commercial AFM can perform measurement with a pixel density of 512×512 or 1024×1024 pixels. Because some animal cells present dimensions that needs scans on area of 100μm×100μm, this implies that any single pixel covers approximately an area of 100nm×100nm for a pixel density of 1024×1024. For this reason, the increasing of resolution can play a fundamental role for the recognition of cells patterns or organ shapes. Figure 4 presents an image of a large osteocyte. The primitive image is low resolution, 512×512 pixels on an area 50μm×50μm, after LR to HR method is applied, the 3D reconstruction presents all the characteristics features as in the 2D AFM image
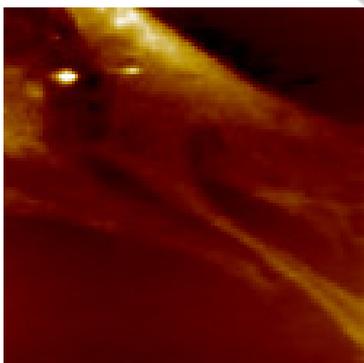

Figure 4: AFM image of a portion of an osteocyte (real area surface 50μm×50μm, z-height less than 5μm, density pixel 512×512).
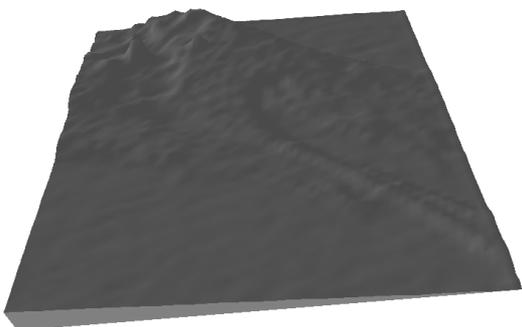

Figure 5: The correspondent 3D reconstruction of the osteocyte as in figure 4.

In many cases, another problem generally found during the imaging of cells is the identification of specific cells in a cluster. In fact, in a cell culture, the differentiation is often followed by meiosis, so producing a population of cells partially overlapping one each other. This is the case of the adipocytes displayed in figure 6. Two nuclei are well recognized, but it is not so for the cell edges. The 3D reconstruction can help to identify cells dimensions and organs in a manner that is not possible in the 2D image and correspondent three-dimensional visual rendering performed both with open source (Gwyddion, http://gwyddion.net) or commercially available programs (SPIP, http://www.imagemet.com)

Figure 6: AFM image of a cluster of adipocytes (real area surface 50μm×50μm, z-height approximately 8μm, density pixel 512×512).
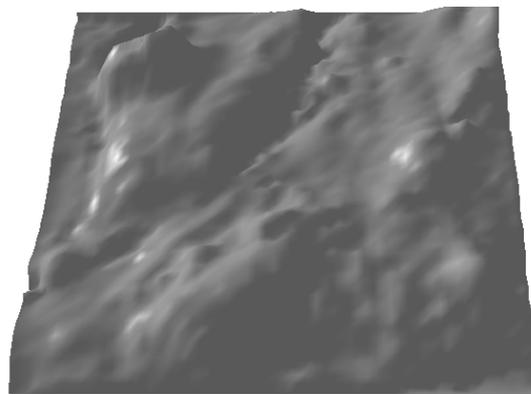

Figure 7: 3D reconstruction of the cluster cells as in figure 6. The cells structures are well defined, it is possible to recognize the nuclei.

5 CONCLUSIONS

Atomic Force Microscopy (AFM) is a fundamental

tool for the investigation of a wide range of mechanical properties on nanoscale due to the contact interaction between the AFM tip and the sample surface. The information recorded with AFM is stored and synthesized by imaging the sample properties to be studied. The AFM topographic images are matrices $z=f(x,y)$, that links a z-value to the correspondent x,y surface point. The focus of this paper is on an algorithm for the reconstruction of 3D structures extracted by typical 2D surface AFM images. The AFM images resolution is limited by the tip-sample convolution due to the combined geometry of the probe tip, density pixels and specific the pattern configuration of the sample. This limited resolution reflects on the accuracy of the correspondent 3D image. We have adopted an inferential procedure that provides a high-resolution algorithm for the single-image AFM raw data and then the construction of a 3D routine for the improved resolution images. When applied to cell populations, the 3D reconstruction are an useful tool for the recognition of cell pattern and organs and it could be used for a fast *in situ* analysis for biologists and biomedical scientists.

REFERENCES

Altmann S. M., Lenne P. F., Horber H., 2000. *Rev. Sci. Instrum.,* 72, 142-149.

Amit Y., Grenader U., Piccioni M., 1991. J. Amer. *Statist. Assoc.* 86, 376-387.

Amit Y., 1994. *SIAM J. Sci. Comput.,* 15, 207-224.

Belikov S., Shi J., Su C., 2008. *American Control conference Seattle Washington,* USA, ThA08.5 (1-5).

Beyder A., Spagnoli C., Sachs F., 2006. *Rev. Sci. Instrum.*, 77, 1551-7.

Clayton, G. M., Devasia, S., 2005. *Nanotechnology* 16, 809–818.

D'Acunto M., Salvetti O., 2011, *Pattern Recognition and Image Analysis*, 21, 9-19.

Danti, S., D'Acunto M., Trombi L., Berrettini S., Pietrabissa A., 2007. *Macromolecular Bioscence*, 7, 589-598.

Flores F. C., de Alecar Lotufo R., 2010. *Image and Vision Computing*, 28, 1491-1514.

Gonzalez, R., Wood, R., 2008. *Digital Image Processing. Upper Saddle River*, NJ, Prentice Hall.

Hardie R. C., Barnard K. J., Armstrong E. E., 1997, *IEEE Transactions on Image Processing*, 6, 1621-1633.

Henn S., Witsch K., 2000. *Computing*, 64, 339-348.

Henn S., Witsch K., 2001. *SIAM J. Sci. Comput.*, 23, 1077-1093.

Hug H. J., Yung T., Güntherodt H. J., 1992. *Rev. Sci. Instrum.*, 63, 3900-3904.

Pickup L. C., Capel D. P., Roberts S. J., Zissermann A., 2009. *The Computer Journal*, 52(1), 101-113.

Tipping M. E. Bishop C. M., 2003. In Becker S. Thrun S. and Obermeyer K. (Eds.), *Advances in Neural Information Processing Systems*, 15, 1303–1310.

Torrez-Mendez L. A., Ramirez-Sosa Moran M.I., Castela M., 2007. In *Gelbuck A., Kuri Morales A. F., MICAI 2007, LNAI 2007*, 640-649. Springer-Verlag Berlin Heidelberg.

Yurov, V. Y., Klimov, A. N., 1994. *Rev. Sci. Instrum.*, 65(5) 1551-7.